Performance of the CHAPS Collectors

J.S. Coventry
Centre for Sustainable Energy Systems
Australian National University
Canberra 0200 A.C.T.
AUSTRALIA
E-mail: joe.coventry@anu.edu.au

Abstract

The performance of the Combined Heat and Power Solar (CHAPS) collectors at the Australian National University is described. Results from testing of the collector under steady state conditions at a range of input temperatures are presented. Measured results under typical operating conditions show thermal efficiency around 57% and electrical efficiency around 11%, and therefore a combined efficiency of 68%. An energy balance for the CHAPS collector is carried out, showing the relative significance of optical and thermal losses. The thermal performance of the collector is examined in detail, using temperature measurements within the receiver and at the glass surface. The transmission and absorption properties of the cover materials across the solar spectrum are examined using a spectrophotometer. Using these results, the temperature profile of the receiver is modelled using the finite element package Strand7. The results are discussed, and in particular, methods suggested for reducing the large temperature gradient between the centre and outside edges of the solar cells.

INTRODUCTION

The Centre for Sustainable Energy Systems (CSES) at the Australian National University (ANU) has developed a photovoltaic/thermal (PV/T) collector with geometric concentration ratio of 37x. The so-called Combined Heat and Power Solar (CHAPS) collectors consist of glass-on-metal mirrors that focus light onto high efficiency monocrystalline silicon solar cells to generate electricity. Fluid flowing through a conduit at the back of the cells removes most of the remaining energy as heat, which can then be used for building heating and domestic hot water. The first commercial installation of single-axis tracking CHAPS technology is a 300m^2 system providing electricity, and domestic and heating hot water for Bruce Hall, a residential college at ANU, with construction commencing in November 2003.

DESCRIPTION OF THE CHAPS SYSTEM

The development of the CHAPS systems was preceded by PV trough technology development at the ANU since the mid-1990s, culminating in the commissioning of a 20kW two-axis tracking passively cooled PV trough array at Rockingham, Western Australia (Smeltink et al., 2000). Since then efforts have focused on actively cooled CHAPS systems designed for integration in buildings to supply hot water and electricity. The collectors are made up of 1.5m long mirror and receiver modules, which are connected end-to-end to form a row. The first CHAPS prototype is a single trough, 15m long, pictured in figure 1. The Bruce Hall system is made up of 8 troughs, each 24m long. The mirror, receiver and solar cell widths are 155cm, 8cm and 4cm respectively, which gives a geometric concentration ratio of 37x excluding the shading due to the receiver.

Figure 1. Prototype CHAPS collector at ANU.

The solar cells manufactured by CSES (figure 2), are monocrystalline silicon cells designed to have low internal series resistance, since the high current density under concentrated radiation significantly affects the fill factor of the cell. Low series resistance around 0.043 Ocm^2 is achieved in the ANU concentrator cells by a) narrow spacing of the conductive fingers, which reduces the distance electrons travel through the silicon, b) heavy phosphorous doping beneath the fingers to reduce the contact resistance and c) a relatively large electroplated silver finger cross-section. Most cells are around 20% efficient at 25°C under 30 suns concentration.

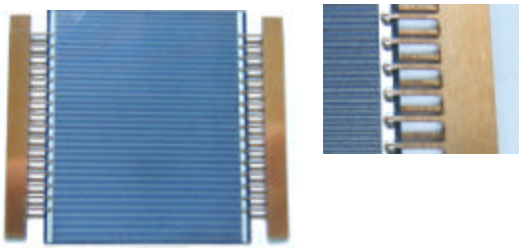

Figure 2. ANU concentrator cell.

The solar cells are bonded to an aluminium receiver with a thermally conductive, electrically insulating tape. They are connected in series and encapsulated with silicone and low-iron glass. Schottky bypass diodes are used to protect the cells against going into reverse bias due to partial shading of the receiver. The heat transfer fluid, which is water with anti-freeze and anti-corrosive additives, is pumped through the extruded aluminium receiver (figure 3) to cool the cells and collect thermal energy. The back and sides of the receiver are insulated with 20mm thick glasswool encased by a galvanised steel cover. Internal fins have been incorporated in the fluid conduit to increase the heat transfer surface area in order to minimise the operating temperature difference between the cells and the fluid.

Figure 3. Cross-section of the ANU receiver.

The parabolic mirrors were developed at the ANU by Glen Johnston and Greg Burgess, and follow on from similar development of three-dimensional curved mirrors for dishes (Johnston et al., 2001). The glass-on-metal laminate (GOML) mirrors are composed of a silver backed mirror 1mm thick, laminated to a sheet metal substrate. The mirror is held in its parabolic shape by stamped tab ribs at either end

of the mirror. The glass surface is highly scratch resistant when compared to some plastic film concentrators, and the mirrors have been subjected to a number of years of accelerated lifetime testing without significant deterioration.

The sun-tracking controller, designed at the ANU (Dennis, 2002), controls a linear actuator that is connected to a circular tracking wheel by cables. The tracking accuracy is set to ±0.2°. Because of the stamped tab rib design, there are small gaps between the mirrors averaging around 19 mm. To achieve good shape accuracy with a GOML mirror, it is desirable to have a continuous sheet across the width, and therefore the receivers are supported from outside the mirror. The support arms and mirror are mounted on a single square section beam designed to have a maximum of 0.5° twist along its length.

EXPERIMENTAL APPARAT US AND METHOD

The thermal and electrical performance of a CHAPS receiver was measured using a custom built outdoor testing unit (figure 4).

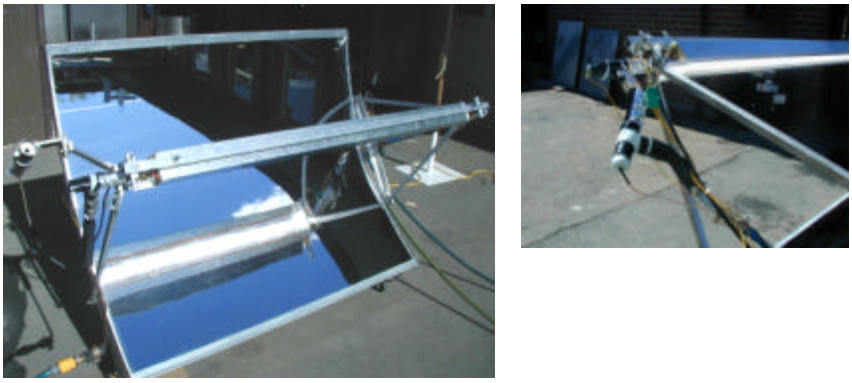

Figure 4. Outdoor testing unit.

The 125cm wide trough is narrower than on the prototype system, but a little longer than the receiver to ensure an even radiation flux distribution along the length. The test receiver is made up of 28 cells connected in series, one of which is bypassed due to failure upon installation. The cells average 16.8% efficiency at 65 degrees under 30 suns flux intensity. The cells were chosen to have similar maximum power point currents.

Parameters measured include the direct beam radiation, measured with a Kipp & Zonen pyrheliometer, the ambient temperature, measured with a PT100 probe mounted in a Stevenson's screen, the wind speed and direction, the inlet temperature of the water, measured with a PT100 probe inserted into the flow, the temperature difference across the collector, measured using a differential thermocouple arrangement, and the mass flow, measured with a calibrated turbine meter with ±1% accuracy. The mass flow was held near 40 ml/s for all the tests. Inlet temperature was held constant with either a mechanical tempering valve or temperature controlled booster heater. The data was sampled across 4 days, with wind speeds ranging from 0 – 0.6 m/s and the receiver angle varying from around 45º to 70º from horizontal.

A resistive load was held across the receiver at the maximum power point. The load was set at a defined voltage, and adjusted to the maximum power voltage by regular comparison with IV curves measured from the receiver. The voltage was measured across the receiver, and current measured across a current sense resistor. A DataTaker DT600 was used for the data logging. Data was logged every 10 seconds, and returned each minute. The trough was tracked manually to face directly at the sun at all times.

EFFICIENCY RESULTS

The thermal output $\dot{Q}_{th}$ and electrical output $\dot{Q}_{elec}$ of the CHAPS collector are calculated from the measured data as follows:

$$\dot{Q}_{th} = c_p \cdot \dot{m} \left(T_{out} - T_{in}\right) \quad (1)$$

$$\dot{Q}_{elec} = I_{mp} \cdot V_{mp} \quad (2)$$

where c_p is the specific heat at the average fluid temperature, $\dot{m}$ is the mass flow, and T_{out} and T_{in} are the outlet and inlet temperatures respectively of the fluid. I_{mp} and V_{mp} are the current and voltage of the receiver at the maximum power point. The thermal efficiency h_{th} and electrical efficiency h_{elec} are calculated based on the following definitions:

$$h_{th} = \frac{\dot{Q}_{th}}{\dot{G}_d \times A_m} \quad (3)$$

$$h_{elec} = \frac{\dot{Q}_{elec}}{\dot{G}_d \times A_m} \quad (4)$$

where $\dot{G}_d$ is the direct beam radiation and A_m is the product of the mirror width of 125cm, and length of 150cm. Note that the receiver aperture is actually only 143.5cm long, so the efficiency measure includes losses due to hydraulic connections at the ends of the receiver, as well as losses due to the shading caused by the receiver itself.

Figure 5 shows the efficiency results for the receiver when it is operating both with and without an electrical load. T_m and T_{amb} are the mean fluid temperature and ambient temperature respectively.

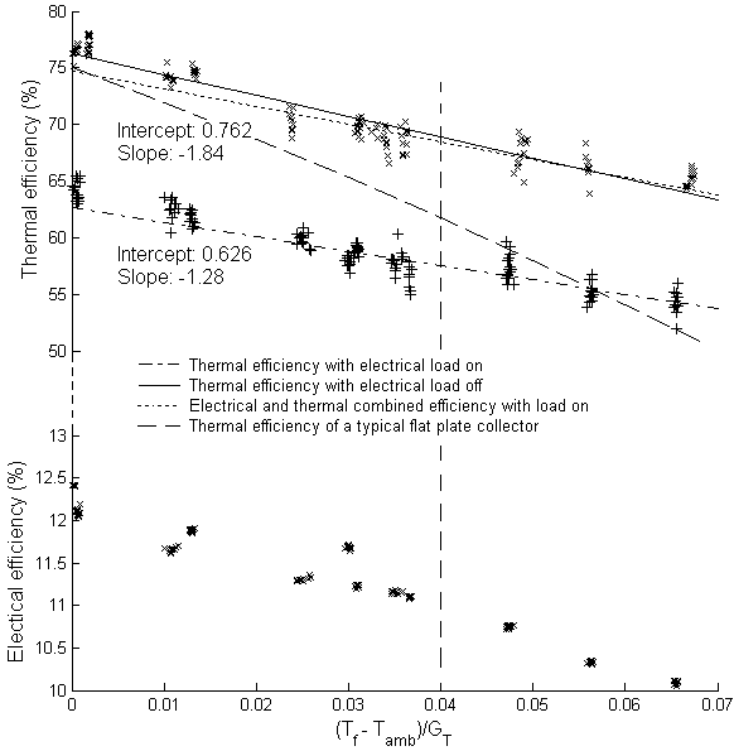

Figure 5. Efficiency curves for the CHAPS receiver.

The electrical efficiency is plotted on the same scale in order to show the data points corresponding to the thermal efficiency data points. However, the electrical efficiency depends on absolute temperature

rather than temperature difference. Addition of the electrical efficiency data to the thermal efficiency data yields a combined efficiency trend very similar to that of the thermal efficiency when there is no electrical load.

The thermal efficiency compares well with other technologies designed to operate at a similar temperature. Under typical operating conditions of, say, fluid temperature of 65ºC, ambient temperature of 25ºC and direct radiation of 1000 W/m^2 (shown by the vertical line on figure 5), the CHAPS collector has thermal efficiency of 57% and electrical efficiency of 11%. The efficiency curve for a typical flat plate collector is superimposed on figure 5, and shows a thermal efficiency of 62% under the same operating conditions. The overall energy conversion for the CHAPS collector is higher, and 11% electrical conversion is equivalent to a good quality flat plate PV system under operating conditions.

OPTICAL PERFORMANCE

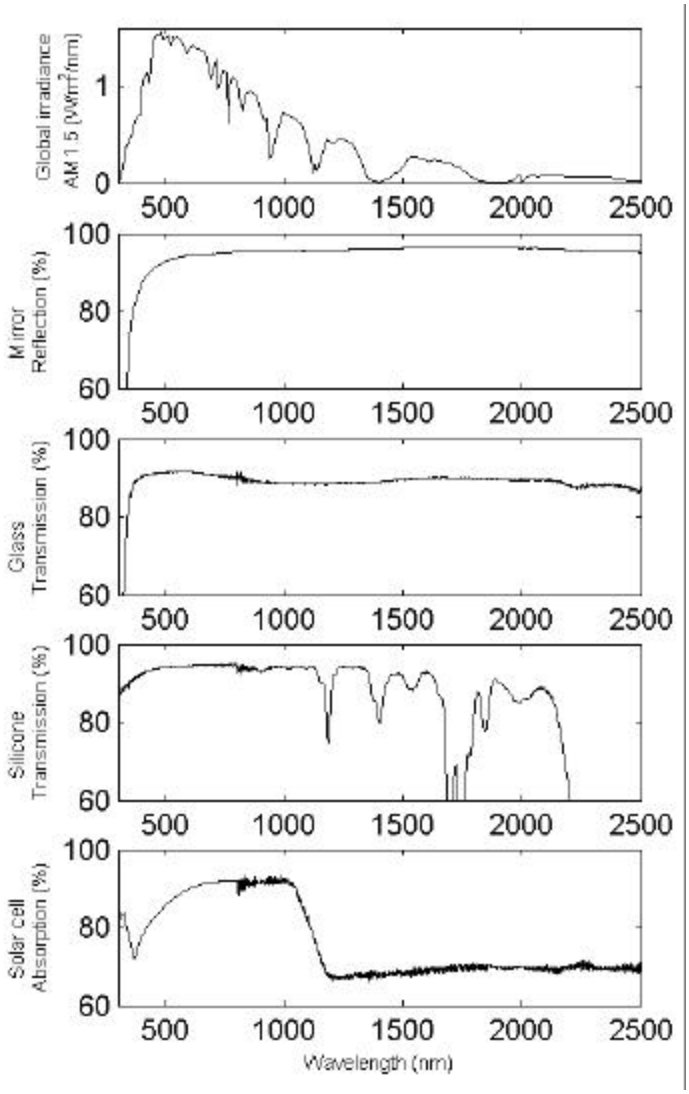

Figure 6. Spectrophotometer measurements of the key optical components of the CHAPS system

A Cary 5 spectrophotometer was used for spectral measurements of transmission, reflection and absorption for the various components of the CHAPS collector. The spectrophotometer consists of a

110 mm diameter integrating sphere that collects most reflected or transmitted radiation, removes directional preferences, and presents an integrated signal to a detector. The measurement is compared to 0% and 100% baseline measurements to determine the percentage reflected or transmitted. The spectrophotometer was used in the spectral range 300 – 2500 nm. The spectral dependence of the mirror, glass, silicone and silicon solar cell, has been measured and the results presented in figure 6. Weighted average figures for reflectance, transmission and absorptance are weighted by the global irradiance at AM1.5. Therefore optical properties in the visible region (approx. 400-700nm) are more heavily weighted than in the ultraviolet region or near infrared.

The mirror has a weighted average reflectivity of 93.5%. Reflectivity actually peaks at 96.5% at 1.7µm, but there is minimal solar radiation in this region. The cover glass is reasonably transparent above 400nm, and has a weighted average transmissivity around 90%, including reflection losses at both the front and back air-glass interfaces. The spectral reflectivity curve for the silicone potant also includes losses from two silicone-air interfaces. The transmissivity of silicone is very good between about 400 – 1100 nm, however at higher wavelengths, distinct absorption bands can be seen. These bands correspond to excitation frequencies for the covalent bonds within the silicone compound. Because the heat flux due to absorption in the cover materials in the centre of the focal beam is significant, the transmissivity of both glass and silicone was measured for a wide range of thicknesses t in order to determine the absorption coefficients K according to Bouger's law:

$$\frac{I_t}{I_0} = e^{-Kt}$$

where I is the local radiation intensity. The plot of weighted transmissivity for various thicknesses of silicone and glass is shown in figure 7. The extinction coefficients for the glass and silicone potant are calculated as 0.0046/mm and 0.010/mm respectively. Therefore the absorption that could be expected in the 3.3mm thick Starphire glass is 1.5%, and for the 2mm thick silicone, 2.0%.

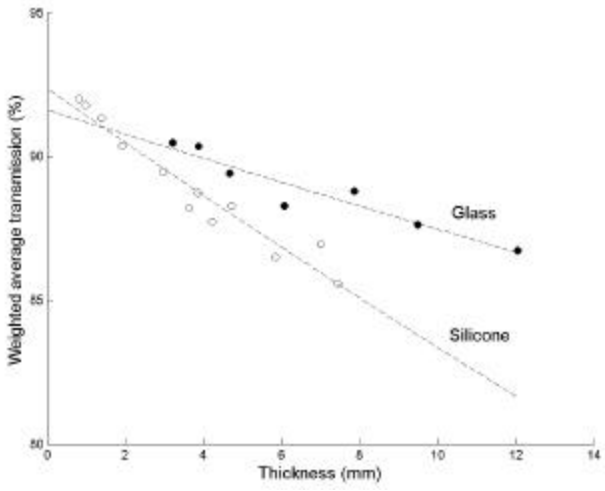

Figure 7. Weighted average transmission for various thicknesses of glass and silicone

In a receiver, there is intimate contact between the glass, the silicone potant and the cells. Therefore, there is one air-glass interface, one glass-silicone interface, and one silicone-silicon interface. Silicon has a relatively high refractive index (peaking at short wavelengths at about 6.5, which accounts for the spike in figure 8, and levelling out at about 3.6), and therefore it is quite reflective. To improve the light trapping, cells are textured to allow the reflected light a second opportunity to enter the cell, and to allow light to be retained within the cell through total internal reflection. Figure 8 shows the reflectivity of a cell before and after encapsulation. The weighted reflectivity of the cell is reduced from 15.9% to 11.4% when it is encapsulated. Despite the extra absorption in the cover glass and potant, the light that escapes from the cell has the opportunity to be reflected back to the cell from the inside surface of the glass, and because the surface of the cell is textured, most of the light that escapes the cell exits at an angle sufficient for total internal reflection at the glass-air interface.

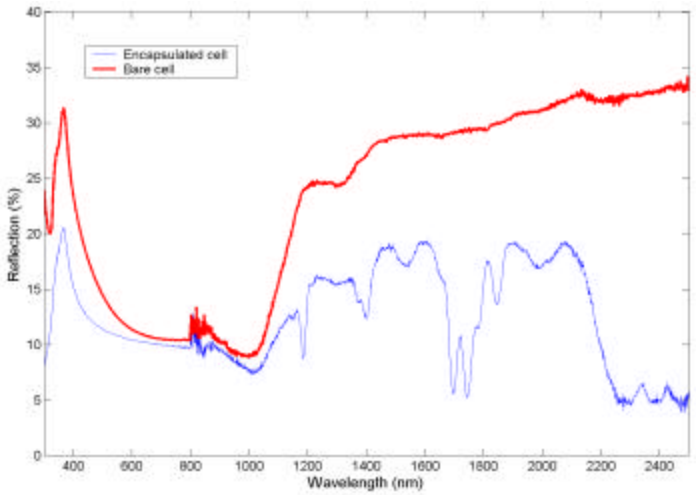

Figure 8. Reflectivity of a cell – before and after encapsulation

ENERGY BALANCE

Losses from the collector can be termed as optical losses, electrical losses, or thermal losses. Optical losses include mirror absorption, mirror shape error, and reflections from the receiver. Thermal losses include convection and radiation losses from the cover glass, and conduction losses through the insulation surrounding the rest of the receiver. Electrical losses within the receiver are manifested as heat. The voltage of the receiver is measured close to the ends, and therefore external voltage drops in cabling and other electrical components can be neglected. The following analysis uses results from the test rig introduced above for steady state tests on 21 October 2003. Results of the energy balance and key parameters for the test are shown in figure 9.

Direct beam radiation	991 W/m^2
Flow	50 ml/s
Inlet temp.	40.7°C
Ambient temp.	23.7°C
Wind speed	0.87 m/s

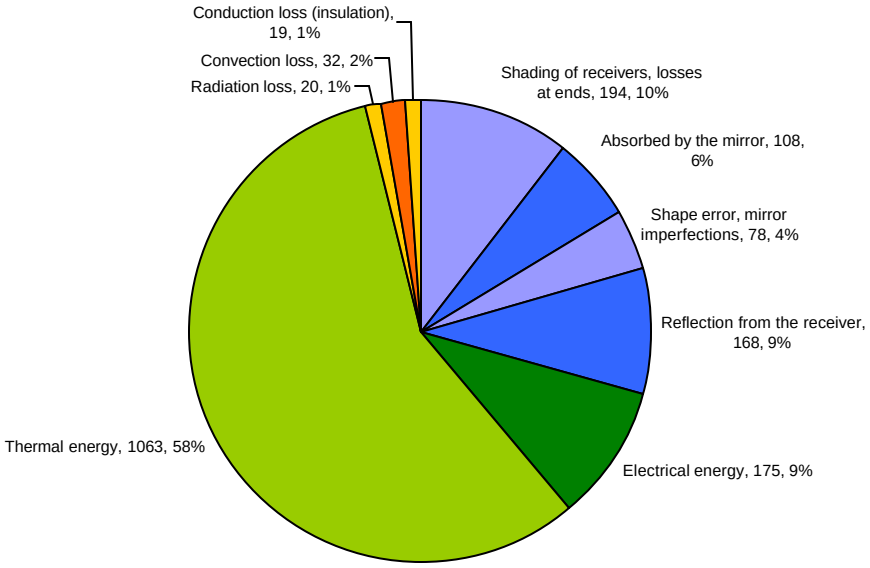

Figure 9. Energy balance for a CHAPS collector, showing energy in Watts, and percentage loss

Optical losses

Optical losses account for 88.6% of the losses in the CHAPS system, and 29.5% of the total energy incident upon the collector. Therefore the optical system has the largest potential for gains in overall

efficiency. Reduction of the gap between receivers through more compact fittings or longer receivers would reduce losses at the ends. Shading losses from the receiver are unavoidable, although will be reduced once the receiver is mounted on the 25% wider mirrors used for the Bruce Hall system. The mirror reflectivity of 93.5% is quite good, although can be substantially reduced by dirt on the mirrors. Cleaning of the mirrors is a necessary part of the maintenance requirements of the collectors. Shape accuracy of the mirrors is estimated as 95%, based on the results of videographic flux mapping carried out by Glen Johnston.

Thermal losses

Due to the relatively small aperture area of the receiver, thermal losses account for only 3.8% of total energy incident upon the collector. For the operating conditions in the above test, convection losses from the glass surface are the main loss. Convection losses depend on many factors such as receiver orientation, wind speed and direction and glass temperature. The losses have been estimated based on calculations of the convection coefficient and measurements of the glass surface temperature using a FLIR Thermacam^{TM} SC2000 thermal camera. Radiation losses and conduction losses through the insulation account for the remainder of thermal losses. Radiation losses are calculated using the measured glass temperature and experimentally determined emissivity of 0.88. The conduction loss coefficient (UA-value) of 0.82 was calculated by insulating the glass surface and measuring the energy loss for known ambient conditions. The UA-value also accounts for losses from the hydraulic fittings at the ends (which were not insulated for the tests).

Thermal and electrical output

The balance between thermal and electrical output changes depending on the quality of the cells, the operating temperature, and importantly, the optical flux profile. The impact on electrical performance of a non-uniform radiation flux profile on a linear concentrator is discussed in detail by Coventry (2003). For this test, one of the bypass diodes was switching on, reducing the efficiency by about 2% compared to the efficiencies shown in figure 5. Electrical energy is generally considered a more valuable form of energy than thermal energy, particularly when the thermal energy is quite low-grade heat (Coventry and Lovegrove, 2003). Therefore, the aim is to maximise the electrical output. This is the main incentive for achieving good heat transfer between the cells and the heat transfer fluid. At present a 0.13mm thin tape with conductivity measured at 0.21 W/m.K is used to attach the cells to the receiver. Other higher conductivity methods of attaching the cells are under trial. The temperature profile within the receiver has been simulated using the finite element analysis software Strand7, as shown in figure 10. The thermal model takes a 2-D slice at the centre of the receiver. Conduction is the fundamental mode of heat transfer between elements in the model, the rate of which is determined by the heat conduction coefficient defined for each different material. Coefficients for convection and radiation are defined at the boundary of the model, as are the surrounding conditions. The model has no capability for computational fluid dynamics analysis, and therefore convection coefficients must be determined for the steady state conditions. The convection coefficient within the receiver is estimated as 756 W/m^2.K based on modification of the Nusselt number for the particular geometry using empirical correlations for turbulent flow in internally finned tubes, developed by Carnavos (Webb, 1987). The heat coefficient for the outer surfaces was set to 8.8 W/m^2.K. Energy can be introduced to the model in two ways: as a heat flux or a heat source. A heat flux is used to model the energy incident upon the solar cells, and is modelled as a Gaussian distribution fitted to the measured flux profile (as measured by Glen Johnston using videographic flux mapping techniques). The heat flux at the cells is adjusted to account for reflection, absorption and the electrical energy conversion. The energy absorbed by the glass and silicone is modelled by assuming there is a heat source within each element, and adjusted to match the experimentally determined absorption rates shown in figure 7.

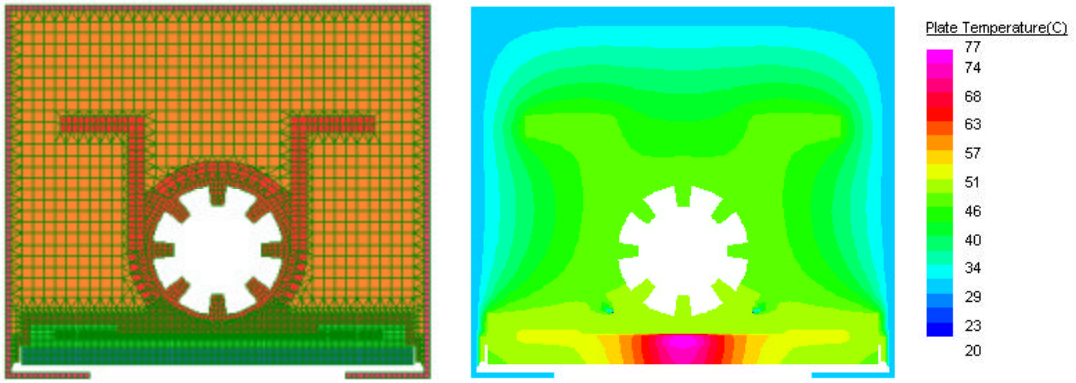

Figure 10. Strand7 model of a receiver showing the finite elements (left) and temperature profile (right).

The above figure shows the impact of the 3.5% absorption in the glass and silicone. Because of the low conductivity of the encapsulating materials, and the very high radiation flux concentration at the centre of the cell, there is a large temperature gradient across the glass and potant. The temperature profile of the surface of the glass midway along the length of the receiver is plotted in figure 11, along with the temperature calculated by the Strand7 simulation. The simulation under-predicts how hot the glass actually gets. Modelling shows that the glass temperature is most sensitive to the conductivity of the thermal tape, and the absorption in the glass and silicone. As discussed above, total reflection from an encapsulated cell is reduced compared to a bare cell because of the total internal reflection of light from the inside of the glass surface. Therefore, some of the light that is bouncing around inside the glass and potant will be absorbed, and the path length of the light through these materials will be increased by the angles that light exits the textured silicon. Therefore absorption is likely to be significantly more than 3.5%. The dashed lines in figure 11 indicate the effect of increased absorption on glass temperature. However, because thermal losses from the glass surface are relatively small, the operating temperature of the silicon solar cell remains essentially unchanged (as shown on the right in figure 11) despite the increase in glass temperature due to absorption. The amount of light available for electrical conversion is reduced by the absorption, although for the silicone potant, most of the absorption is in the infrared and therefore doesn't affect the solar cell performance.

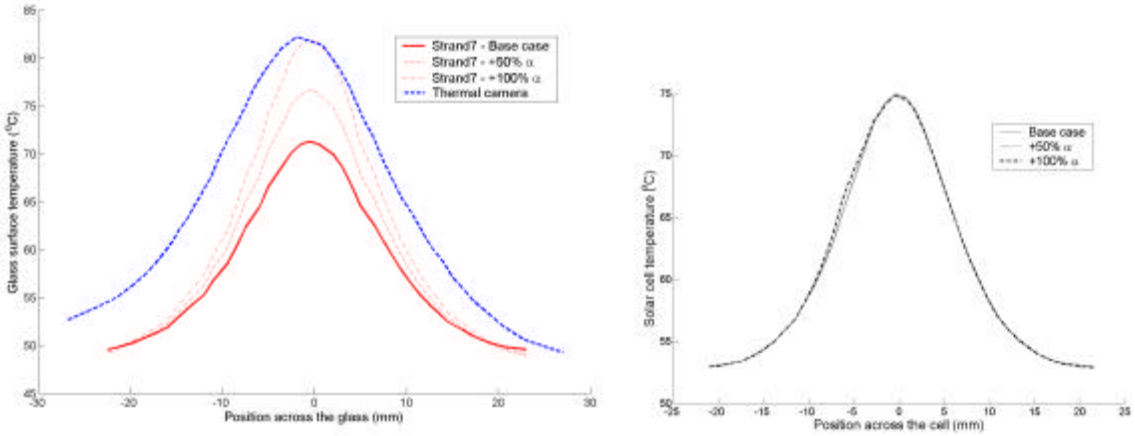

Figure 11. Comparison between glass temperatures measured with the thermal camera, and simulated in Strand7 (left) and the impact of absorption on cell temperature (right).

Improvement of the conductivity of the means of attaching the cells to the receiver has the most potential to significantly reduce the cell temperature. Strand7 modeling indicates that an increase in conductivity of the material with the same thickness to 1 W/m.K would decrease the average cell temperature by around 8°C, and decrease the temperature at the centre of the cell by as much as 12°C.

CONCLUSIONS

Testing of a CHAPS collector has shown thermal efficiency around 57%, and electrical efficiency around 11% under typical operating conditions. Most of the energy lost is due to optical losses. The balance between thermal energy and electrical energy depends primarily on the quality of the cells, optical flux profile and the operating temperature. Most important to the cell temperature is the conductivity of the material bonding the cells to the extrusion. While absorption in the cover materials is significant and increases the temperature of these materials, the negative impact on the electrical performance is not large. The CHAPS collectors will soon be tested on a larger scale (300 m^2) at Bruce Hall, a residential college at ANU, with construction commencing in November 2003.

REFERENCES

Coventry, J. S., 2003: An investigation of non-uniformities in the longitudinal radiation flux profile of a single-axis tracking parabolic trough concentrator. *ANZSES Solar Energy Conference*, Melbourne.

Coventry, J. S. and Lovegrove, K., 2003: Development of an approach to compare the 'value' of electrical and thermal output from a domestic PV/thermal system. *Solar Energy*, **75,** 63-72.

Dennis, M., 2002: The ANU Sun Tracking Controller - User Manual (available on request at the ANU), Australian National University.

Johnston, G., Burgess, G., Lovegrove, K., and Luzzi, A., 2001: Economic Mass Producable Mirror Panels for Solar Concentrators. *ISES Solar World Congress*, Adelaide.

Smeltink, J., Blakers, A., and Hiron, S., 2000: The ANU 20kW PV/Trough Concentrator. *16th European Photovoltaic Solar Energy Conference*, Glasgow, 2390-2393.

Webb, R. L., 1987: Enhancement of Single-Phase Heat Transfer. *Handbook of Single-Phase Convective Heat Transfer*, S. Kakac, R. K. Shah, and W. Aung, Eds., Wiley-Interscience.